Research Article | Vol. 32, No. 17 / 12 Aug 2024 / Optics Express 30756
Optics EXPRESS

Downconversion master slave optical coherence tomography for simultaneous *en-face* imaging at two depths

RAMONA CERNAT, ALEJANDRO MARTINEZ JIMENEZ, AND ADRIAN PODOLEANU*

Applied Optics Group, School of Physical Sciences, University of Kent, Canterbury, CT2 7NH, UK
ap11@kent.ac.uk

Abstract: We report the production of two *en-face* optical coherence tomography (OCT) images from two different depths in real time, using three interferometers in a configuration of double downconversion master slave OCT. Two active mixers are used to produce the analog product of two photodetection signals. A low-cost digitizer with a sampling rate just at the level of twice the inverse of the tuning interval is used, with a much lower sampling rate than that required by the conventional A-scan-based OCT imaging at the same tuning rate. Not employing a fast digitizer for the photodetected signal, as conventional OCT imaging does, the selection of temporal windows from the photodetected signals is achieved by low-cost RF switches. Optimum conditions for the active mixers and switches employed are evaluated to optimize the downconversion operation.

1. Introduction

OCT was invented in 1991, by adding a lateral scanner to a low coherence interferometer [1]. The modern and fastest type of OCT technology is based on the generic diagram shown in Fig. 1, where the optical source is a tunable laser, a swept source. This implements Fourier domain or swept source (SS)-OCT [2,3] and performs depth interrogation by spectral analysis of the optical signal at the OCT interferometer output [4]. A spectrum interrogator made from a fast photodetector and a fast digitizer. A Fourier transform (FT) block processes the digitized electrical signal delivered by the photodetector to obtain an A-scan (a reflectivity profile in depth in the sample imaged). The spectrum interrogator and the FT block play the role of a decoder, to infer spatial information from the spectral encoding of optical path difference in the interferometer into a specific modulation of the spectrum. The photodetected signal is proportional to the spectrum modulation at the interferometer output, that due to interference is channeled, referred from now on as a channeled spectrum (CS). The entire A-scan is computed from a FT of the entire CS, delivering P points of reflectivity, A_1, A_2, ... A_p, ... A_P, delivered along a single output.

A majority of SS-OCT systems on the market employ swept sources at 100 kHz and there are numerous research reports that show that for retina imaging, even sweeping at a few MHz rate can deliver a decent signal to noise ratio image with power to the eye below the safety level [5]. An expensive component of the system in Fig. 1 is the digitizer sampling the photodetected signal. Increasing the sweeping rate demands larger sampling rates that puts extreme demands not only on the digitizer speed, but on the handling of enlarged data size.

To illustrate the requirements for data handling demanded by using faster sweeping tunable lasers, let us consider an interferometer with a single reflector in each arm, determining an optical path difference (OPD). Within a bandwidth $\Delta\lambda$ of the spectrum of the optical source, with

#530325 https://doi.org/10.1364/OE.530325
Journal © 2024 Received 17 May 2024; revised 11 Jul 2024; accepted 17 Jul 2024; published 9 Aug 2024

Optics EXPRESS

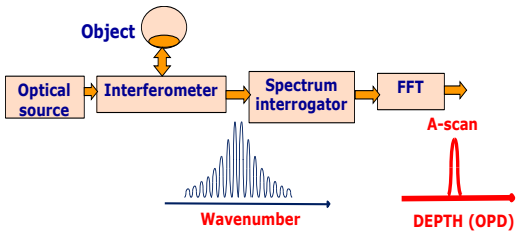

Fig. 1. Block diagram of a SS-OCT system.

central wavelength λ, the output spectrum becomes modulated (channeled) by a number of peaks (cycles), given by $N \sim OPD\Delta\lambda/l^2$. As λ^2/Dl defines the axial resolution, N signifies the number of resolvable points in depth. For a tuning rate of 1 MHz and N = 1000 (a typical value in OCT), the bandwidth of the photodetected signal exceeds 1 GHz, demanding a digitizer with at least 2 GS/s sampling rate, with a cost exceeding $10,000. With a trend in an ever increasing the sweeping rate, digitization becomes an expensive part of the OCT technology [6].

An alternative to the conventional method of using a high frequency rate digitizer was presented in a previous report, based on downconversion master slave OCT (DMS) [7]. This reduced the demand for the sampling rate of the signal employed by a N/2 factor. As another advantage of the downconversion method, is the direct provision of *en-face* OCT images. In opposition, employing a conventional OCT system as described in Fig. 1, based on a FT processor, all A-scans for all lateral pixels need to be acquired, followed by assembly of the A-scans into a volume of the object. Only then a software cut of the volume at the depth required delivers the *en-face* OCT slice. This takes some time, especially if the sweeping is nonlinear and on each sweep, resampling is necessary [8,9].

In [7], the digitizer used was of a high end, 1.8 GS/s ultra-fast sampling board due to the need to compare the DMS operation with that of a conventional OCT system in Fig. 1 based on digital sampling of the photodetected signal. In this paper, the digitizer serves the scope of DMS only, hence the sampling rate needed is largely relaxed to the level of twice the inverse of the tuning time interval.

DMS introduced in [7] is based on hardware, real time calculation of a A(p) point of the A-scan via multiplication of the two photodetected signals from the master and the slave interferometers. Multiplication is secured using an analogue mixer. The point in depth, p, in the object placed in the object arm of the slave interferometer is selected by the optical path difference in the master interferometer.

In general, in all SS-OCT systems, the fast digitizer part of the spectrum interrogator block, also performs cropping of the signal to eliminate the edges of the sweep where tuning is profoundly nonlinear. As no fast digitizer is employed after the photodetector, in this report we show how trimming of the right part of the sweep can be accomplished by fast switches, using electronic circuitry that is a small fraction of the cost of a fast digitizer otherwise employed in the conventional OCT diagram in Fig. 1. This procedure, using switches and presented here, brings advantages in terms of the signal to noise ratio in comparison with the first report on DMS [7].

In addition here, DMS-OCT is demonstrated on two simultaneous *en-face* OCT channels. The two *en-face* OCT images are produced online, while the incident beam is laterally scanned over the target. The depths where the two images are obtained from can be changed by operating on the optical path difference in each of the two master interferometers.

Furthermore this paper demonstrates how technology of fast active mixers can achieve better performance than passive mixers initially used in [7] in terms of cross talk between the inputs and the output and sensitivity on the two inputs.

Optics EXPRESS

The process of multiplication of the signals produced by the Slave interferometer with the signal produced by the master interferometer is subject to random fluctuations of phase difference between the two signals. Therefore, here the paper presents a further improvement to the DMS method, consisting in using active I&Q mixers. The proper conditions of employing such devices are presented in comparison with the conditions of using passive simple mixers as reported in the previous report [7].

2. From FT based OCT to master slave OCT and then to downconversion OCT

In conventional FT based spectral OCT, the decoder in Fig. 1 performs a FT of the electrical signal corresponding to the channeled spectrum, *C(k)*, where *k* is the wavenumber. For a tuning bandwidth between a minimum k_m and a maximum k_M, at a certain axial coordinate *z* along the depth in the sample, the backreflected strength is given by:

$$A(z) = \sum_{k_m}^{k_M} C(k) \cdot e^{i \cdot k \cdot 2z} \tag{1}$$

where *2z* is the OPD in the interferometer. An A-scan *A(z)* is delivered over all sampled points *z* along depth in the sample, via the FT using the monochromatic basis functions (the exponential terms) of different periodicities dictated by *z* over the spectral coordinate *k*. In master slave (MS) OCT [10,11] the numerical calculation in (1) is changed to:

$$A(z) = \sum_{k_m}^{k_M} C(k) \cdot e^{i[g(k) \cdot 2z + h(k)]} \tag{2}$$

where *g(k)* represents the dependence of tuning rate on the wavenumber *k* and *h(k)* the dispersion left uncompensated in the interferometer.

Both conventional FT based OCT processing and MS numerical processing employ a digitizer to handle a number n of samples in the wavenumber k of the channeled spectrum, C(k), during the sweeping time τ. Fast numerical processing is employed by both methods to perform the multiplication of the *C(k)* with the exponential basis of functions in (1) and (2). In fact in FT based conventional spectral OCT, a modified version of data *C(k)* (a resampled set of data) is employed to correct data for the effects described by *g(k)* and *h(k)* [8,9]. In (1) the exponential is monochromatic while in (2) polychromatic, due to the chirping imposed by variation of *g(k)* and *h(k)* on the wavenumber *k*.

In downconversion MS OCT (DMS) [7] employed here, according to the MS protocol, data is left as it is received. This means that both factors in (2) are chirped. However, in DMS the multiplication is performed by an analogue multiplier followed by a low pass filter with a low cut off frequency ~ 2 /t. In addition, in DMS, for the depth of interest determined by the coordinate *z*, the exponential in (2) (a chirped oscillation) is generated live using a master interferometer driven by the same swept source as the slave interferometer (equipped with the lateral scanner and collecting data *C(k)* from the sample).

In the present study, two master interferometers are used to generate *en-face* images from two depths in the sample placed in the sample arm of the Slave interferometer as dictated by the optical path differences in the two master interferometers.

3. Experimental set-up

The system employed for this study is schematically presented in Fig. 2. A swept source (SS), from Axsun Technologies, 1060 nm central wavelength, tuning at 200 kHz over a bandwidth of 111 nm (982-1093 nm) at 10 dB is employed. The light at the SS output is split by a fiber splitter 5/95 with 95% towards a slave Interferometer (SI) and 5% sent towards a fiber splitter sending 50:50 to two master interferometers (M1I and M2I). In the object arm of the slave interferometer, a dual galvanometer scanning head (Cambridge Technology, GXY 6210 Series Galvanometer

Optics EXPRESS

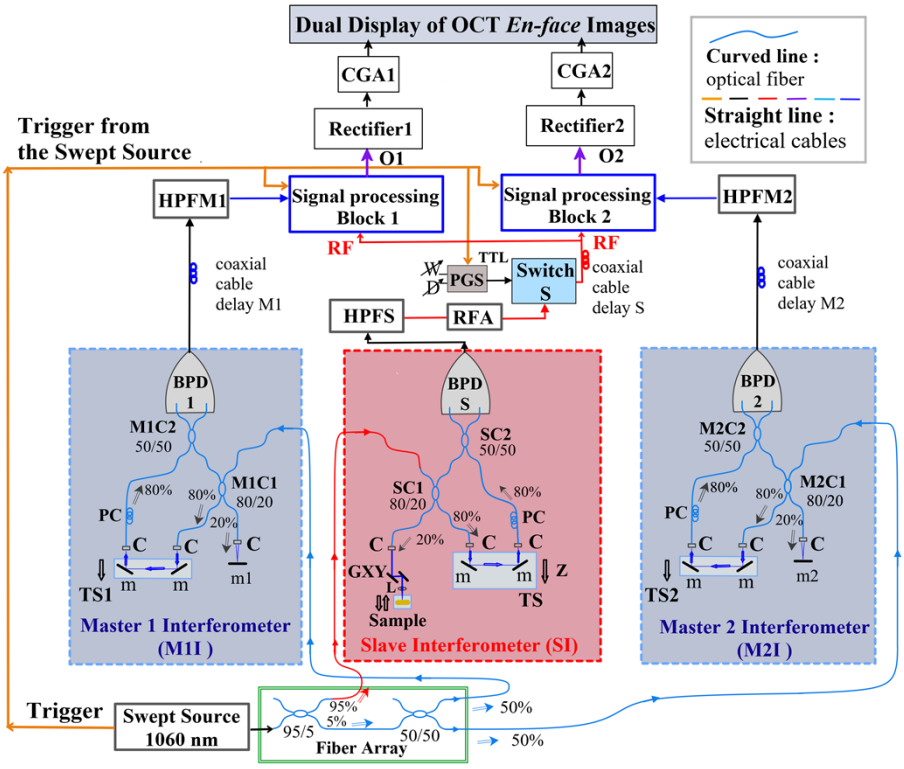

Fig. 2. Schematic diagram of the experimental set-up: SC1, M1C1, M2C1: 20/80 fiber couplers; SC2, M1C2, M2C2: 50/50 fiber couplers; M1I, M2I: Master interferometers; SI: Slave interferometer; BPDS, BPD1, BPD2: balanced photo-detectors in the Slave, M1I and M2I interferometers respectively; TS, TS1, TS2: translation stages; m, m1 and m2: metal flat mirrors; GXY: orthogonal galvanometer scanners; C: collimators; HPFS, HPFM1, HPFM2: high pass filters; L: lens; C: collimators; PGS: pulse generator driving Switch S; D: adjustment of the output pulse delay; W: adjustment of the output pulse duration; TTL: Transistor-Transistor-Logic signal to synchronize Switch S; CGA1, CGA2: Contrast and Gain adjustment blocks; HPFS, HPFM1, HPFM2: High pass filters for SI, M1I and M2I; RFA: radio frequency amplifier; O1, O2: outputs of the Signal Processing Blocks 1, 2; PC: polarization controller.

scanners) is used to scan the optical beam over the sample, via a lens L. In each interferometer (SI, M1I and M2I), light is split into a sample arm and into a reference arm using 20/80 couplers SC1, M1C1 and M2C1 respectively. The two waves from the reference and sample arms in the three interferometers are combined in 50:50 fiber couplers SC2, M1C2, and M2C2 respectively. Light from fiber is collimated to free space by New Focus aspheric lenses, C, *x10* (15.3 mm focal length) apart from that collimating light to the scanning head in the slave interferometer, which is x20 (8 mm focal length). The outputs of these interferometers feed three identical balanced photo-detectors BPDS, BPD1 and BPD2 (Thorlabs, Model PDB481C, AC 30 kHz −1 GHz). High pass filters (HPFM1, HPFM2, HPFS), with a cut-off frequency of 6.7 MHz (Thorlabs, Model EF513) are used at the output of all balanced photo-detectors to eliminate the direct current (DC) and the low frequency variations of the photo-detected signals due to power variation during sweeping. At the output of the HPHS, signal is further amplified by a radio frequency amplifier, RFA, 0.1-1000 MHz, 18 dB gain (Mini-Circuit ZFL-1000-VH2+). Adjustment of optical path difference in each interferometer is performed via translation stages

Optics EXPRESS

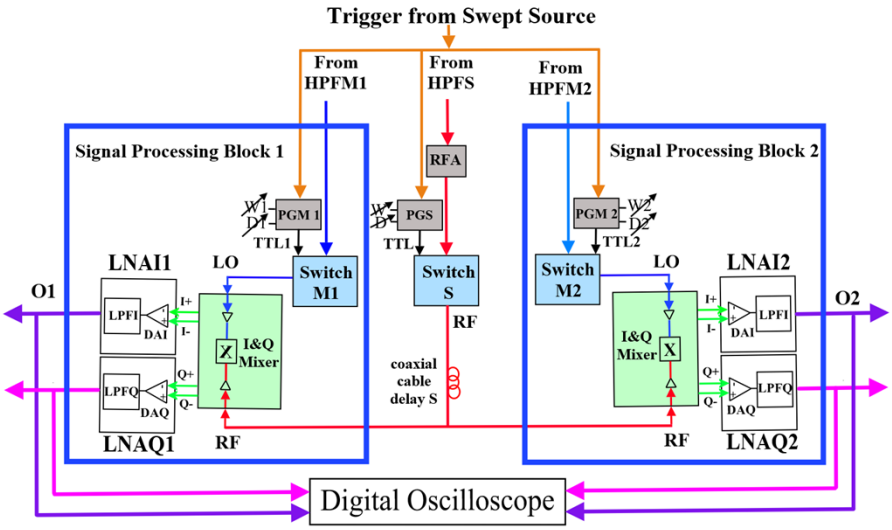

Fig. 3. Schematic diagrams of the two signal processing blocks 1,2; HPFS, HPFM1, HPFM2: High pass filters for Sl, M1I and M2I; D, D1, D2: adjustment of pulse duration; W1, W2: adjustment of pulse width; PGM1, PGM2, PGS: pulse generators; RFA: radio frequency amplifier; X: active mixer; I+, I-, Q+, Q-: output signals of the active mixers; DAI, DAQ: differential amplifiers; LNAI1, LNAQ1, LNAI2, LNAQ2: low noise amplifiers; LPFI, LPFQ: low pass filters; DAI, DAQ: Differential amplifiers; RF: mixer radiofrequency signal input; LO: local oscillator mixer input; TTL1, TTL2: Transistor-Transistor-Logic signals to synchronize Switches M1 and M2; O1, O2: outputs of the Signal Processing Blocks 1, 2.

TS, TS1, TS2. TS in the SI is controlled by a micrometer motorized stage (Newport MM4006) while the other two translation stages in M1I and M2I are manual. Distance travelled by the translation stage TS is shown as z, this is also equivalent to the depth (measured in air) in the sample arm, where the optical path difference is $2z$.

Figure 3 presents the schematic diagram of the signal processing blocks in the two channels: signals from the output of SI and M1I interferometers, and the signals from SI and M2I interferometers are sent to two identical direct conversion quadrature demodulators acting as active mixers (analog devices, LTC5584, 30 MHz to 1.4 GHz frequency range). The signals from these two mixers are gated by two switches (minicircuits, ZASWA-2-50DRA+) controlled by the SS trigger. Three signal generators (Hewlett Packard HP8112A, 50 MHz), PGS, PGM1 and PGM2, are used to produce pulses of adjustable width, W, W1, W2, under controllable delays, respectively D, D1, D2. The switches allow selection of the most useful parts of the sweep to be used to create the images.

The outputs of each of the mixers X1 and X2 are electrically amplified (Stanford Research, LNA SR560) (LNAI1, LNAI2, LNAQ1, LNAQ2). Such LNA kits are equipped with gain amplifiers, differential input and low pass filters, LPFI and LPFQ that are set to 1 MHz. The two LNAI1 and LNAI2 are used to amplify the difference of signals of I+ and I- and two other LNAQ1 and LNAQ2 are used to amplify the difference of Q_+ and Q_- signals. For characterization of each active mixer, all of its 4 outputs are used via two LNAs as shown in Fig. 3 and (a) digital scope, employed to perform the calculation [7]:

$$X = \sqrt{(I_+ - I_-)^2 + (Q_+ - Q_-)^2} \tag{3}$$

For imaging, we did not have resources (4 LNAs and two extra digitisers) to perform the calculation in (3). Hence for imaging we have used the outputs O1 and O2 of the low noise

Optics EXPRESS

amplifiers, LNAI1 and LNAI2 (i.e. signal I from the mixers only). As shown in Fig. 2, signals from O1 and O2 are fed to two integrated circuit rectifiers (analog devices AD637), Rectifier1 and Rectifier2 followed by analogue blocks to control the contrast and the gain, as well as to amplify the signal, CGA1 and CGA2 respectively (Rectifier1,2 and CGA1,2 are own assembled circuits with potentiometers to adjust contrast and gain of the images displayed). The CGA1,2 outputs are sent to the inputs of a digitization and data processing board (National Instruments, PCI-6132) placed in a PC used to display two images simultaneously (Dual Display of OCT *En-face* images). There is a 2nd card in the PC that controls the scanners (National Instruments PCI-6221). An in-house software produces two images simultaneously, each of 512×512 pixels in synchronism with the triggers from the signals driving the scanners in the slave interferometer.

Power from the swept source is 15 mW, power in the sample arm in the slave interferometer is 1.5 mW, while to mirrors m1 and m2 in the master interferometers M1I and M2I is 0.04 mW and 0.034 mW respectively. Power in the reference arms after the 80/20 couplers SC1, M1C1 and M2C1, in front of mirrors m on the reference stages TS, TS1 and TS2 are respectively: 8 mW, 0.2 mW, 0.14 mW. Powers are less than those estimated using the coupling ratios of 5/95 or 20/80, as in several places, FC/APC adapters are used (i.e. fiber is not continuously spliced).

4. Active versus passive mixers

An improvement was introduced in implementing downconversion here in comparison with the previous report [7], where a passive mixer (minicircuits ZFM-4, 5-1250 MHz) and a passive I&Q demodulator (Minicircuits ZFMIQ-10D, 9-11 MHz) were used. Here, two direct conversion quadrature demodulator active mixers (analog devices, LTC5584 30 MHz to 1.4 GHz frequency range) are employed.

There are several improvements brought by using active mixers. The main improvement in comparison with using passive I&Q demodulators is their much wider band of operation. For instance using minicircuits ZFMIQ-10D in [7], the bandwidth was only 2 MHz around 10 MHz. Another advantage that refers even to their operation as simple mixers (i.e. using either I and Q only as output) is that the LTC5584 employs an amplifier for the signal from the local oscillator (LO) input. This leads to two improvements:

(i) Lowering leakage between the signals applied to the two mixer inputs, RF (signal from the slave OCT channel) and LO (signal from the master OCT channel). The leakage using passive mixers was ~ -25 dBm for ZFM-4 and -60 dBm for ZFMIQ-10D while the AM used here exhibits -80 dBm (at 450 MHz);

(ii) Amplification on the LO input, that within a sufficiently wide range of OPD values, makes the mixer output less dependent on the signal strength from the master channel. This is also particularly important here due to the division of power towards 3 interferometers, i.e. less power per each interferometer in comparison with [7]. Having amplifiers on the LO inputs allows sending more power to the SI and less to the M1I and M2I, hence the first coupler ratio of 95/5, i.e. the M1I and M2I receive ~ 2.5% only of the swept source power.

The passive mixers are based on transformers and balloons and use bridges of diodes. The output of a passive mixer, within its limits of operation, is more or less proportional to the amplitudes of signals at their inputs. As another improvement the output amplitude of an active mixer is strictly proportional to the amplitude of signal applied to the RF input. This is in addition to the better tolerance to the LO input signal strength. As the intention was to use the LO inputs for the photodetected signal provided by photodetectors in the master interferometers, we assessed this behavior in order to quantify the active mixer output variation on the strength of signal provided to the LO input. Increasing the OPD, the interference signal strength decreases. However, the active mixers are expected to provide less output variation with amplitude at the

Optics EXPRESS

LO input than their passive counterpart due to their limiting amplifier on the LO input. In other words, we expect a more constant output when increasing the OPD in the master interferometer with the intention to combat the amplitude decay with OPD. However, the limitation of amplitude introduces new harmonics and limits the axial range usable, as explained further down.

First, we characterized the LO input of the active mixers. As for the 200 kHz Axsun source, the photodetected signal RF bandwidth is from a few tens of kHz to 1 GHz as demonstrated in [7], tests were performed on using signal generators applying sine signals within such bandwidth. The mixers were measured using two signal generators at 101 MHz to the LO input and at 100 MHz to the RF input. The amplitude of the frequency difference of 1 MHz signal at the I_+ output was measured for variation of the amplitude signal applied to the LO input from 3 mV to 30 mV, for three amplitudes of the signal applied to the RF input (10 mV, 100 mV and 500 mV). Very similar curves were obtained for both active mixers, with results presented in Fig. 4. The curves in Fig. 4(a) show saturation of output for amplitudes larger than 20 mV for RF values below 100 mV, and the curve in Fig. 4(b) show a saturation level of ~ 70 mV for RF values of 500 mV.

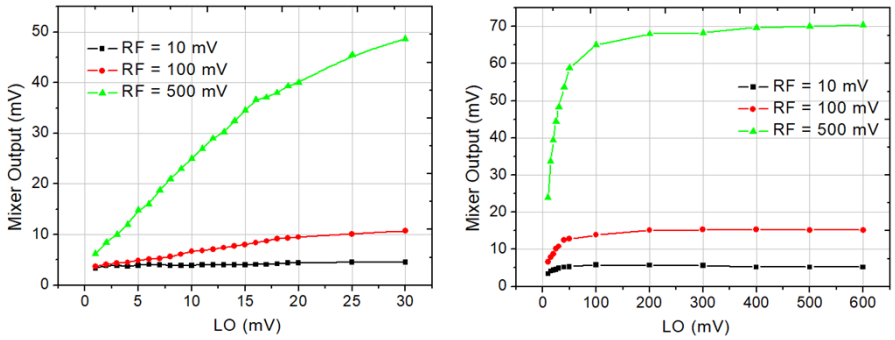

Fig. 4. Dependence of the active mixer output I_+ versus amplitude of the signal applied to the LO input (to be connected to the output of the balanced photodetector in the Master interferometer) for small amplitudes (a) and for large amplitudes (b).

Then, we characterized the RF input for both types of mixers using two signal generators at 100 MHz and at 101 MHz. For comparison, due to the RF bandwidth targeted, we could not use a passive I&Q, hence the simple passive mixer ZFM-4 was used. The amplitude of the frequency difference signal was measured for variation of the amplitude signal applied to the RF input from 10 mV to 600 mV (similar to that expected to be delivered by the balanced photodetector block in the Slave interferometer), whilst the amplitude of signal applied to the LO input was kept fixed at 10 mV, 100 mV and 500 mV (Fig. 5).

Comparing the curves in Fig. 5 show that the output dependence is more linear with RF for the active mixer (Fig. 5(b)) than for the passive mixer (Fig. 5(a)). The curve measured for equal RF and LO amplitudes (blue) simulates the case where a mirror in the slave interferometer is used as sample and advancing similar OPD values in the two interferometers.

The small output amplitude corresponds to the case of large OPD values, where it is known that the interference strength is smaller (sensitivity of SSOCT decays with OPD, [4]). Placing the graphs measured for equal RF and LO amplitudes in the same plane (Fig. 5(c)) comparatively shows that the output decays quicker with RF = LO signal in the passive mixer (Fig. 5(a)) than in the active mixer (Fig. 5(b)). This should positively impact the axial range of the system, where by using an active mixer, larger output amplitudes should be obtained at larger OPD values using an active mixer in comparison with a passive mixer. Using the active mixer, the decay of output with the RF signal exhibits a smaller slope, while for the passive mixer a larger slope. The graphs

Optics EXPRESS

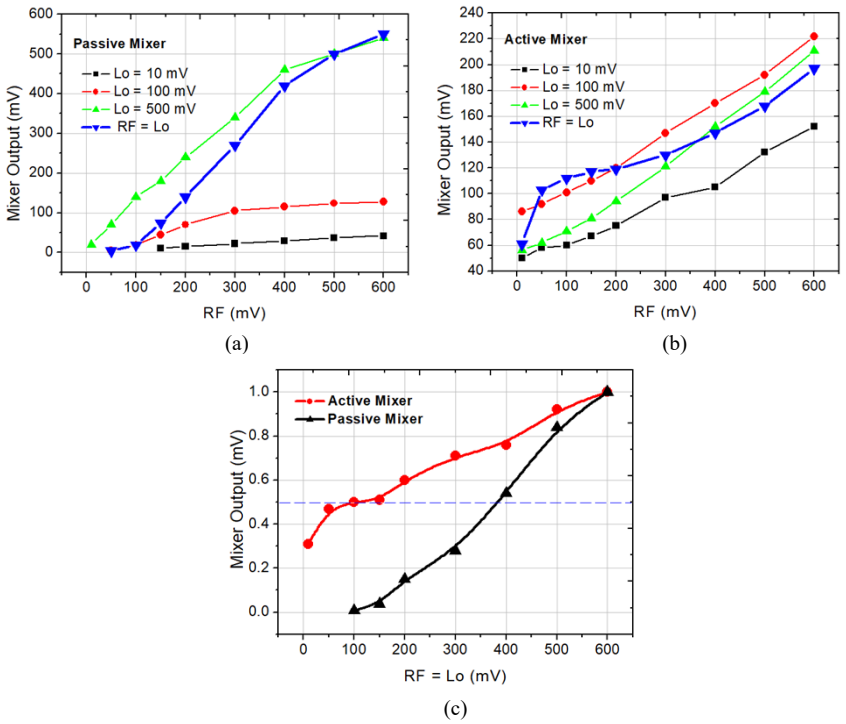

Fig. 5. Dependence of the amplitude of the mixer output versus amplitude of the RF signal for LO fixed at 10 mV, 100 mV and 500 mV for passive mixer (a), active mixer (b) and active versus passive mixer when equal amplitudes, RF = LO (c). The blue curves in (a) and (b) correspond to the curves in (c) where the RF and LO amplitudes are equal.

in Fig. 5(c) illustrate comparatively the improvement potential in the axial range brought by using a limiting amplifier on the LO input, according to graphs in Fig. 4. They show that decay to half amplitude is obtained for a swing of 500 mV using the active mixer while of only 200 mV using the passive mixer (according to the dashed line drown above). The final proof of axial range increase due to using active mixers is documented in Fig. 6(a). Using a mirror as a sample, decay of sensitivity was measured in the Slave interferometer (with some little variations, the curve is similar for the two Master interferometers) versus distance, z, travelled by the translation stage TS in Fig. 2. The strength of the interference signal was adjusted to fit the range of output signal within the linear range of passive and active multipliers, less than 600 mV. This enables evaluation of axial range that leads to reduction of the photodetected signal. These are shown as the horizontal bars marked Passive mixer and Active mixer. For the passive mixer, the output of 410 mV was used, for 200 mV down according to Fig. 5(c). For the active mixer, a 110 mV was considered, i.e. 500 mV down according to Fig. 5(c). At this value the amplifier on the LO input exits saturation.

Considering the measurement of interference amplitude in a single interferometer versus z, as shown in Fig. 6(a), this leads to an axial range Δz of 10.8 mm with the active mixers and 2.5 mm with the passive mixers.

However, the more constant output in relation to variation of amplitude at the LO input should be considered together with the effect of harmonics generation due to the nonlinear amplification of signal at the LO input, as illustrated in Fig. 6(b). For the same conditions as in Fig. 4 left, 100 MHz to the LO and 101 MHz to RF, an RF spectrum analyzer was employed to measure the amplitude of the 1 MHz component. This is generated not only by the difference of frequency

Optics EXPRESS

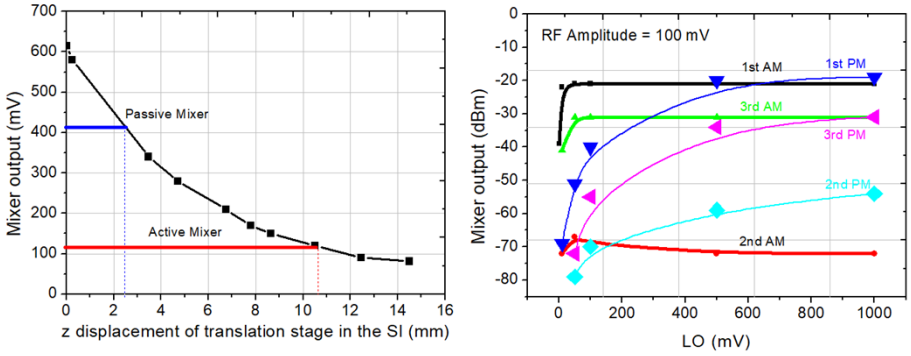

Fig. 6. Illustration of effects due to the amplitude of signal at the LO input. (a) Decay of sensitivity with OPD/2 in the Slave interferometer. The two horizontal bars represent the axial range enabled by the passive (blue) and active (red) mixers; (b) Comparison of 2nd and 3rd harmonic generation behaviour for the passive mixer (PM) and for the active mixer (AM).

of signal on the RF and LO, but also by the difference of multiple frequency components in the RF spectrum when mixed with 200 MHz and 300 MHz, as 2nd and 3rd harmonic of the signal at 100 MHz applied to LO, generated due to limitation regime of the LO amplifier. This means that for an OPD value in the master interferometer, signal will be acquired from the slave interferometer at the similar OPD value as well as from OPD values in the slave interferometer corresponding to harmonics of the signal generated by the master interferometer.

Fortunately, the 2nd harmonic is 40 dB less for the passive mixer (PM) and 55 dB for the active mixer (AM). However the 3rd harmonic is significant, at only 10 dB less than the signal for both PM and AM. This imposes an important limitation to the adjustment of an object along the axial range. If the axial range of the object corresponds to a certain maximum frequency interval f_{max}, with its top placed at OPD = 0, then the only useful axial range free from artefacts due to the 2nd harmonic is the OPD interval corresponding to $f_{max}/2$ to f_{max} and free from 3rd harmonic is the OPD interval corresponding to $f_{max}/3$ to f_{max}. If the OPD is within such intervals, then, a low pass filter with cut-off at f_{max} will attenuate the 2nd and 3rd harmonic image. Considering an object that is placed with its top at an OPD value away from zero OPD, that requires for its axial range an RF range from f_{min} to f_{max}, then to avoid the double of the frequency of the Master generating components within this band, $2f_{min}$ should be larger than f_{max}. Similarly, to avoid the triple of the frequency of the Master generating components within this band, $3f_{min}$ should be larger than f_{max}. Let us consider an object of 2 mm axial range. To avoid the 2nd harmonic, the top of the object should be placed at a z value larger than 2 mm. To avoid the 3rd harmonic, the top of the object should be placed at a z value larger than 1 mm.

4.1. *Delay compensation*

The three interferometers are driven from the same swept source, but via fibers of different lengths. For proper operation of the analogue mixers, the temporal waveforms corresponding to the sweeps should reach their inputs at the same time. Therefore, a delay should be introduced between the slave and master waveforms to correct the mismatch due to the different fiber lengths in the interferometers up to the photodetectors. To compensate for the delay along the fiber, instead of altering the length of fiber, coaxial cables of different lengths are used at the outputs of the three photodetector units up to the switches (Fig. 3) and from switches to the mixer inputs. To perfect such adjustment of coaxial cable lengths, a short optical pulse is created and its transit

Optics EXPRESS

up to the mixer input measured. The swept source is launched into a circulator that guides the light into a FBG centered at 1060 nm in a configuration as shown in Fig. 7.

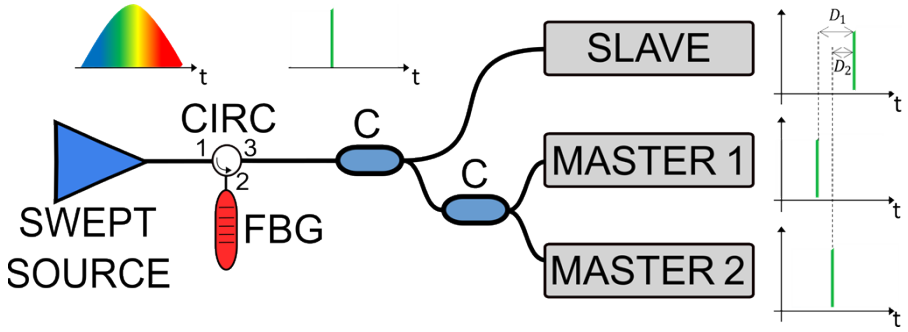

Fig. 7. Schematic diagram for temporal delay mismatching correction.

The short pulse reflected by the FBG is sent to the three interferometers and observed using a fast oscilloscope synchronized by the swept source trigger. To observe the delay of pulses, the sample arms of the interferometers are blocked, and the photodetector units are unbalanced (i.e. one of the fibers is disconnected from one of the photodetectors). Estimation of length adjustment is based on a delay of 1 ns being created by ~20 cm either of fiber or coaxial cable.

Figure 8(a) shows temporal mismatches due to different fiber lengths between channels. Adjusting the connecting cable lengths, pulses are superposed within 100 ps as shown in Fig. 8(b).

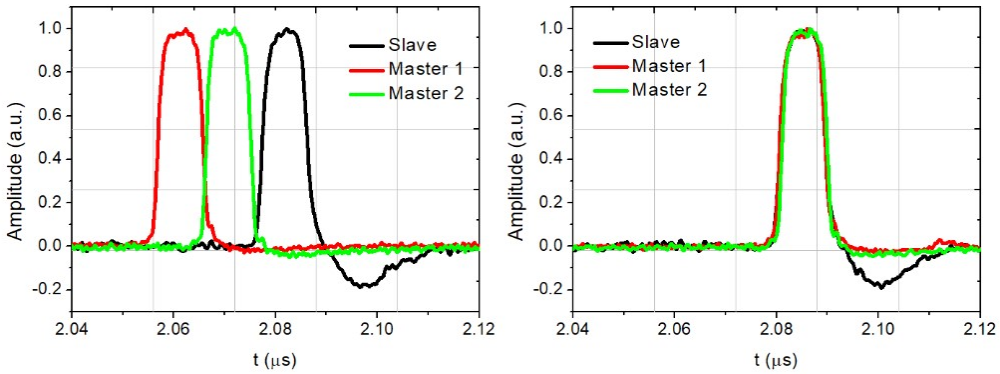

Fig. 8. FBG pulse delays along the three interferometers for (a): Unmatched delays, (b): Matched delay.

Optics EXPRESS

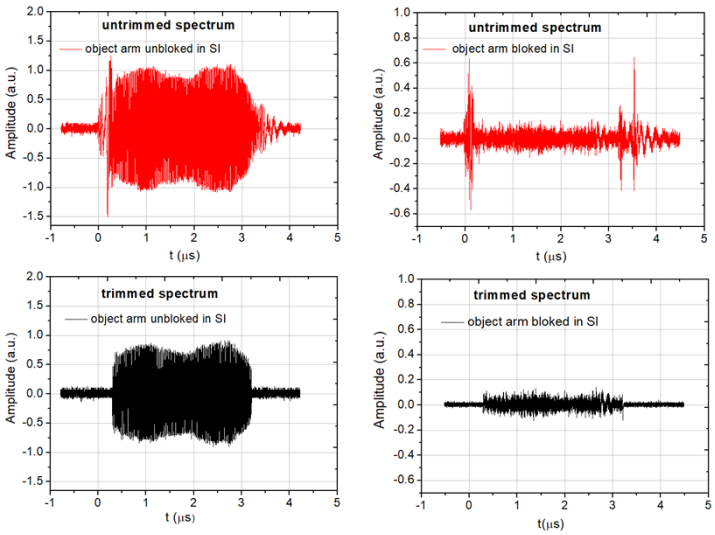

Fig. 9. Interference signal in SI before (top row) and after the SwitchS (bottom row) as displayed by the oscilloscope, using a mirror (left column) and object path blocked (right column).

5. Replacing a fast digitizer with fast switches for trimming of the photodetected signal

In conventional FT based OCT, the fast digitizer is gated in synchronism with the sweeping, in order to eliminate extreme chirps or oscillations at the sweep edges. Here, the excessive chirp due to start and end of tuning device used still needs to be eliminated from the signal processing. Otherwise, downconversion will lead to important DC terms due to low frequency content in the channeled spectra that may not be totally eliminated by the high pass filter used. In the downconversion system used here, the photodetected signals are applied to analogue mixers. Although the frequency of the signal after mixer is much lower, the temporal cropping of length of signal should still be done at the similar rise time and fall time of the fast digitizer, i.e. comparable with the minimum period of the channeled spectrum for an OPD corresponding to the maximum axial range. Therefore, the signals from the two photodetectors in each imaging channel are gated by two fast switches (minicircuits model ZASWA-2-50DRA+) controlled by the SS trigger. For each switch, a Hewlett Packard HP pulse generator (SPG, PGM1, PGM2 in Fig. 3) is used to produce a pulse of adjustable width, W, under a controllable delay, D. The pulse generator allows digital control delay and digital control of the pulse width, enabling precise cropping of the most useful part of each sweep to be employed in image generation. In this way, edge pulses of the sweeps can be eliminated, improving the mixing operation and reducing the non-interference signal coming from the laser pulsations.

The swept source emits above 50% of its peak pulse power for ~ 3.1 μs of the 5 μs period interval. As shown in Fig. 9, edge pulses of the sweeps, with extreme chirps are eliminated by suitably controlling the switches, resulting in gated intervals selected for ~ 2.9 μs. The shorter sweep intervals are similar to those cropped in our systems using high speed digitizer to perform either FFT or MS, for the same reason, i.e. to eliminate the extreme chirps of the sweeping, of large tuning nonlinearity.

Figure 9 shows the interference signal in the Slave interferometer before the SwitchS (top row) and at the SwitchS output (bottom row). The right column shows channeled spectra when the object path is blocked. As shown in the top row left picture, there is a slow oscillating part in the

Optics EXPRESS

channeled spectrum, towards the edges of the tuning interval. These are normally chopped off when using a fast digitiser for either FFT with resampling or for numerical MS. When the object path is blocked, this oscillating part continues to exist, showing that it is not due to interference and hence contributes to reduction of the S/N ratio. The bottom row right spectrum is obviously quieter after eliminating the edges of the channeled spectra. Using the delay D and pulse width W controls on the pulse generator PGS in the slave interferometer PGS, channeled spectra were cropped as detailed above, slightly affecting the axial resolution, but with the advantage of better S/N obtained.

Figures 10 and 11 illustrate the effect of using switches on signals obtained after the active mixers. Signal displayed is that of Eq. (3) using signals from the SI and M1I trimmed using controls D, W on PGS and D1, W1 on PGM1. Trimming the spectra affects little the amplitude of the output signal, but eliminates the secondary lobes. The figures show the secondary lobes in the M1I even at a large distance, 0.4 mm away from maximum, trimmed down by proper control of SwitchM1 and SwitchS. Figure 10 shows the relative amplitude of spurious signal, in red, of significant signal, of ~1/4 from the maximum, in comparison with the useful signal (black), illustrating the need for trimming in order to achieve good S/N and good axial resolution.

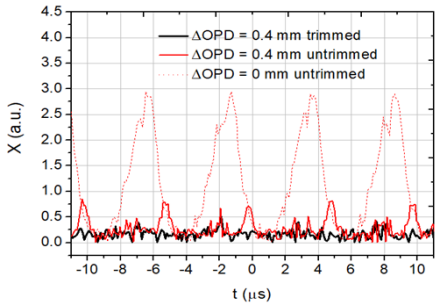

Fig. 10. Mixer output signal, X, measured using signal from the M1I, for an OPD value where maximum signal is obtained (dotted red) superposed over the same signal 0.4 mm away from maximum, (red continuous line) and after trimming of CS as shown in Fig. 9 left column (black).

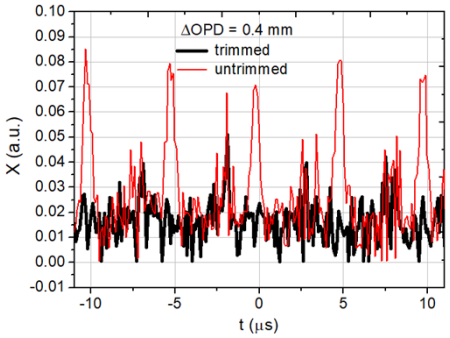

Fig. 11. Mixer output signal, X, measured using signals from the SI and M1I interferometer, at a distance of 0.4 mm from maximum adjusted for DOPD = 0, with untrimming spectrum (red) and after trimming of CS as shown in Fig. 9 bottom row left column (black).

Using a digital oscilloscope, peak to peak values of signal and of noise with the sample arm blocked were measured. With no switches in place, sensitivity was 51 dB, with the switches optimally adjusted to trim the useful part of each spectra, a much better value was obtained, of

Optics EXPRESS

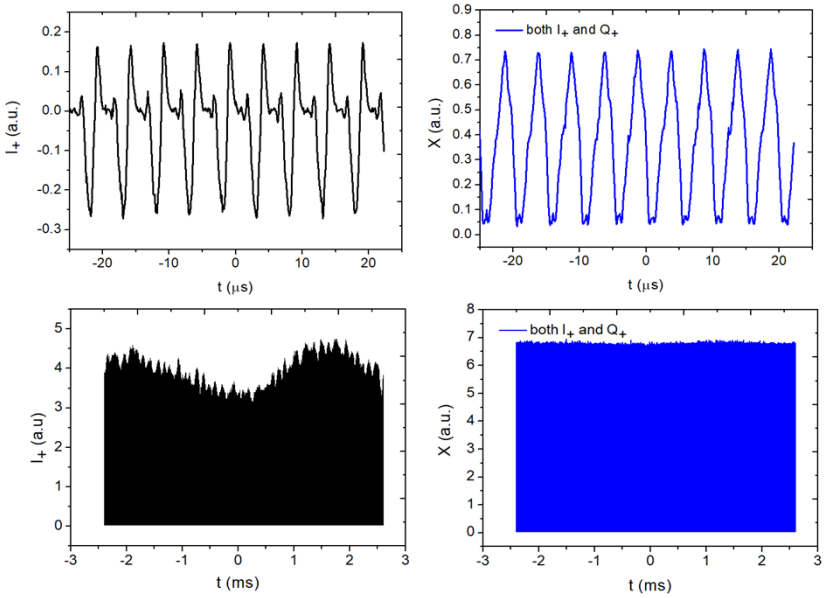

Fig. 12. Stability to relative phase fluctuations in the interferometers obtained by calculating the X signal on a digital scope by using all outputs of the I&Q mixer (right column) in comparison with using a single output, I_+ (left column), equivalent to that obtained using a passive mixer. Top row shows instabilities within the period of the signal, bottom row displays instabilities over a longer time scale of 5 ms.

64 dB. With no switches, the axial resolution presents extended tails, while with the switches in place, the tails are considerably reduced.

In order to display better the attenuation of the residual signal due to using the switches, the two graphs for $\Delta OPD = 0.4$ mm only are reproduced in Fig. 11 with a more sensitive vertical scale.

5.1. Tolerance to phase fluctuations due to I&Q implementation

Figure 12 illustrates the stability to relative phase fluctuations in the interferometers obtained by calculating the X signal when using all outputs of the I&Q mixer in comparison with using a single output, I_+. The later would be equivalent to the behaviour shown by using a passive mixer. Top row shows instabilities over a short time scale while the bottom row displays instabilities over a longer time scale.

6. System characterization

The parameters of the two OCT channels are in line with those communicated in the previous report [7]. Due to the amplifiers in the active mixers, the lower power in the master interferometers than in [7] has not affected the sensitivity significantly. In terms of axial resolution, this is 35 μm when using M1I and 32 μm when using M2I, similar to the values previously reported. The poorer axial resolution was commented in [7] as due to different dispersion in the SI in comparison to that in M1I and M2I. The lower sensitivity than that expected for a MS procedure (using masks obtained from the same interferometer employed as master and as slave sequentially for calibration, respectively imaging), was explained in [7] as due to the higher noise of downconversion. Low frequency components as well as deterministic modulations in the optical source, not sufficiently attenuated by balance detection and high pass filters, contribute to noise.

Optics EXPRESS

As a compromise between lateral resolution and Rayleigh range, an achromat of 3 cm focal length was used as lens L. This, together with a collimator of 8 mm focal length determined a transversal resolution in the *en-face* OCT images as measured by using a USAF target of ~18 µm. Voltage was applied to the two lateral scanners determining a lateral image size of 2.1 mm, leading to *en-face* images each of 117×117 pixels. The two galvanometer scanners were driven with triangular signals of 500 Hz and 2 Hz across the horizontal axis (line) and respectively vertical axis (frame). Each frame, provided in 0.5 s consisted of 512 interlaced lines. Each frame consisted in two OCT *en-face* images simultaneously displayed.

7. Experimental dual *en-face* OCT imaging

Two procedures of volume inspection are presented: (i) By selecting different path lengths in the reference path of the slave interferometer, the two depths in the sample where images are selected from, are given by the two OPD values selected in the two master interferometers; (ii) Alternatively, OPDs in the slave interferometer and in one of the master interferometer are kept constant and depth in the image produced by the other master interferometer is adjusted by altering its OPD. This may find applications in case a feature is identified at a depth in one of the two images, and the other image is used to explore the volume of the sample above and below that depth.

To guide the imaging, signals from the output of the balanced photo-detectors (BPDS, BPD1, BPD2) are monitored via a radio-frequency analyzer (model HP 8590A, 10 kHz - 1.5 GHz) for the frequency localization of the two depths inside the sample under investigation. For instance, using the conversion factor of 68 MHz/mm [7], the difference of frequencies in the M1I and M2I determine the depth difference between the two slices inspected (considered in air).

The two different capabilities of volume inspection are illustrated by imaging a scorpion, Manchurian type, found in north east China, embedded in a transparent plastic block, as shown in Fig. 13(a), (b) and (c) [12]. The body of the scorpion is divided into two main segments: the prosoma (cephalothorax) and the opisthosoma (abdomen). The opisthosoma is then divided into the mesosoma (preabdomen) of seven segments, which contains most internal organs, and the metasoma (postabdomen) of five segments. The coxae surround a small plate called the sternum. Posterior to the sternum are segments called sternites, the first of which contains the genital operculum, which is a pair of plates covering the genital pore. Posterior to that, on the second segment, are the pectines. These are sensory organs unique to scorpions that aid in locating prey, Fig. 13(d) [13,14].

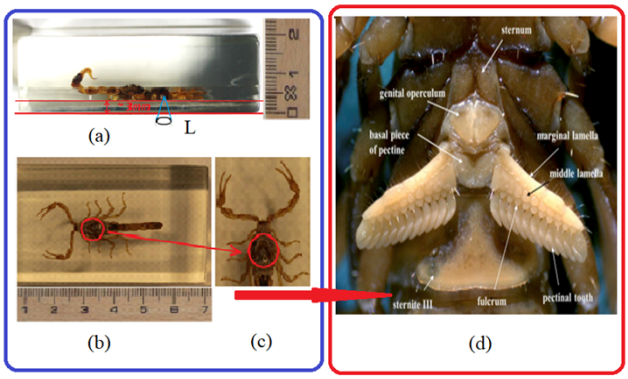

Fig. 13. Photos of the scorpion embedded in a plastic block. (a) Side view: (b) Dorsal view: (c) red circled area is the part imaged in Fig. 14 and Fig. 15 and (d) mesosoma (preabdomen) which contains most internal organs [14].

Optics EXPRESS

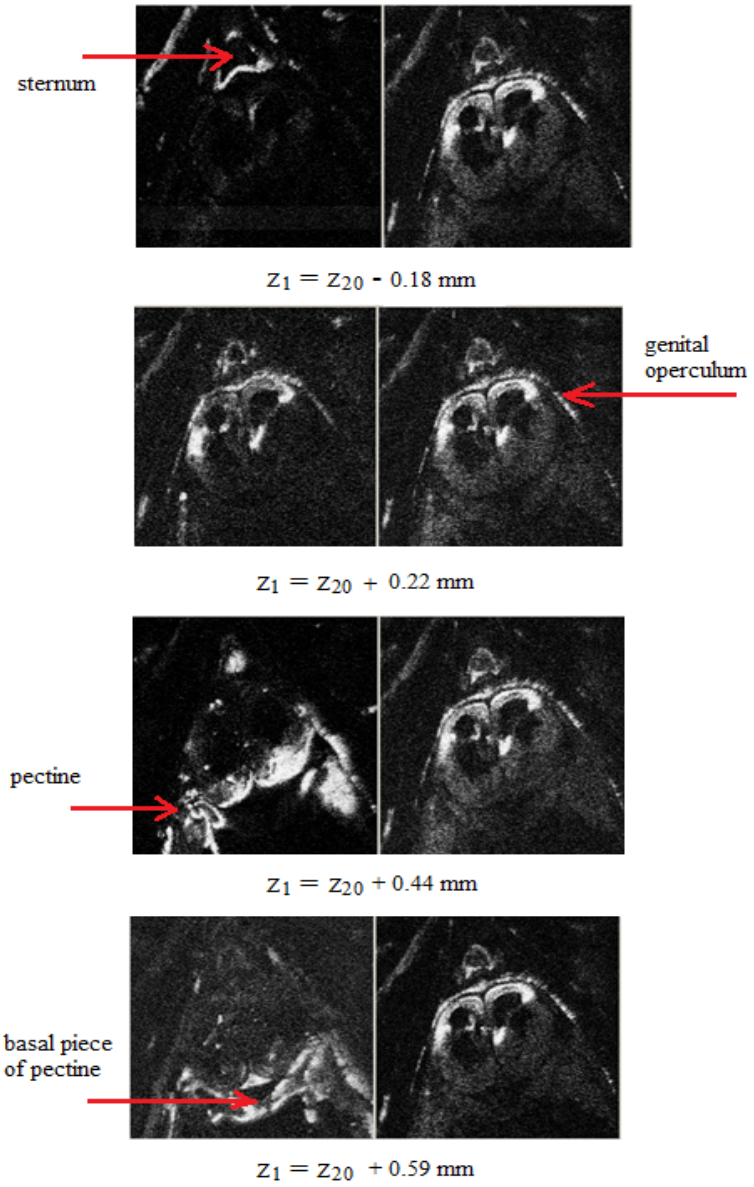

Fig. 14. Dual imaging by varying the OPD in the M1I (left column, using SI and M1I, right column using SI and M2I). Image size 2.1 mm x 2.1 mm.

The sample was positioned and imaged with the stomach facing the lens. The difference in frequency between the top of the plastic slab and the top of the scorpion is 420 MHz. With the conversion factor of 68 MHz/mm this corresponds to a thickness of 6.18 mm measured in air. Using a refraction index n of hard resin of 1.56-1.58, this leads to a thickness of ~ 3.9 mm. This gives ~ 3 mm of plastic for the light to travel and reach the top of the sample. The thickness of the scorpion is ~3.5 mm to image inside the sample.

Optics EXPRESS

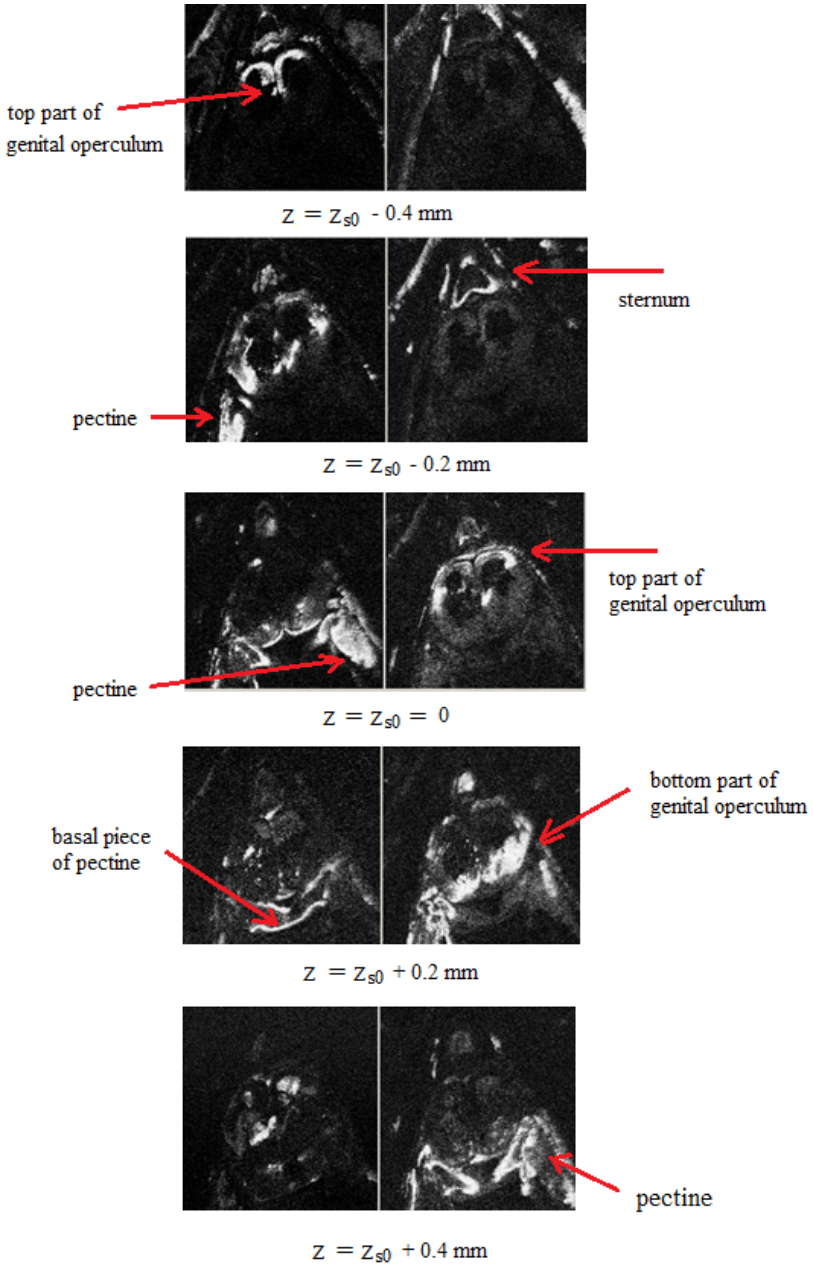

Fig. 15. Dual imaging by varying the OPD = z in the SI. (left column, using SI and M1I, right column using SI and M2I). Image size 2.1 mm x 2.1 mm.

7.1. Holding the OPD in the SI and in the M2I fixed and varying the OPD in the M1I

Figure 14 shows dual *en-face* images, left column, using M1I, varying z_1 while in the right *en-face* images from the same depth, $z_2 = z_{20}$, considered as reference. At the top, the image in the left is below the depth of the image on right, and the next three images are above the depths of the images on the right. The number underneath shows z_1 variation measured in air, as we

Optics EXPRESS

progress from top to the bottom image, sternum, genital operculum, pectine and basal piece of pectine became visible.

7.2. Holding the OPD in the M1I and in the M2I fixed and varying the OPD in the SI

Dual *en-face* OCT images from the scorpion are shown in Fig. 15. A difference of 20 MHz was set initially between the frequencies in the M1I and M2I, corresponding to a difference in z between the two interferometers of 0.29 mm in air. Then the OPD in the SI was changed in steps of $\delta z = 0.2$ mm. The images in the left column are 0.29 mm more superficial than the images in the right column.

8. Conclusions

A configuration of master slave OCT is implemented that can deliver simultaneously two *en-face* OCT images in pixel to pixel correspondence from two different depths in the object investigated. The brightness of each pixel in the images is produced online with the sweeping, i.e. for each spectral sweep, a pixel in the *en-face* image is completed and by the end of lateral scanning, when the 2D frame is completed, the two images are also finalized. The configuration is based on the master slave downconversion principle, where two mask signals (otherwise priorly calculated before acquisition in [11]) are produced live by using two master interferometers, driven by the same swept source employed by the slave interferometer. The masks signals are unique to the depths selected.

The processing hardware takes advantage of the downconversion, where the sampling rate needed to produce each image is at the rate of two times the inverse of the sweeping interval, much lower than the sampling rate needed to sample the modulation of the channeled spectrum. In our case, considering the Nyquist criterion and tuning approximately confined to half period of the swept source emission, for each image, the sampling rate needed is ~ 800 kS/s. Using the same balanced photodetector and the same swept source as in [7], signals of frequencies close to 1 GHz were photodetected and processed by the downconversion method. If conventional processing would be used, sampling rate would need to be at least 2GS/s. This would require a high end digitizer, whose cost exceeds $10 k.

We have discussed and presented the advantage of I&Q active mixers for axial range, amplification of the photodetected signals from the Master interferometers and signal stability. This however would have required a digitizer with 4 inputs, to produce the square of each of the two signals outputs of the I&Q demodulators, followed by square root. Its cost would still be much lower than that of a digitizer required by conventional complex master slave protocol or FFT, exceeding 2GS/s sampling rates. The I&Q mixer performance was documented using a digital scope. For imaging, I&Q demodulation to secure the stability of signal as shown in Fig. 12 could not be harnessed. Hence images obtained and presented could be better in contrast if the full I&Q demodulation capability of the active mixers would have been employed.

A cost analysis shows that electronics circuitry, including an active mixer and a switch are in total less than $300 per channel. For their control, Stanford Research amplifiers were used as differential amplifiers and Hewlett Packard pulse generators, however these could be replaced with simple circuitry whose cost in OEM versions may not exceed $500. In addition, in comparison with FT based OCT and numerical MS based OCT, an extra interferometer and fast balanced photodetector are needed per DMS channel, ~ $2 k. Such costs, in total are a fraction of the cost of a digitizer sampling over 2 GS/s.

Choosing the DMS should be the result of weighing its advantages and disadvantages. Its main advantages are: (i) the direct display of OCT *en-face* images, from as many different depths as the number of master interferometers; (ii) due to downconversion, real time display, i.e. online image delivery becomes possible even for tens of MHz sweeping rates (feasible by using tens of GHz analogue mixers) and (iii) lower cost in terms of digitization. In terms of disadvantages: (i)

Optics EXPRESS

sensitivity is lower than in [7] due to the division of optical power amongst 3 or more Master interferometers, this can be easily addressed by using a more powerful swept source, reduction of power however compensated by the amplification in the active I&Q mixer; (ii) sensitivity is lower than what is expected from a spectral method due to mixing noise associated with the downconversion and deterministic terms not due to interference; (iii) axial resolution affected by dispersion difference between the slave and master interferometers and (iv) multiple images due to harmonics of the signal from the master interferometer, whose avoidance requires reduction of the axial range by half to avoid the superposition with the 2nd harmonic and by third to avoid superposition with the 3rd harmonic. Optimization of dispersion compensation, reduction of deterministic noninterference signals, and more efficient mixers may improve both sensitivity and axial resolution.

As another important advantage, DMS operation can be added to any existing OCT system with two little changes: (i) a diversion of a small fraction of optical power from the swept source to one or more master interferometers, i.e. via a coupler with one or more outputs, with no alteration of the optics or signal processing of the OCT system that in the context of the schematic diagram in Fig. 2, will take the role of the slave OCT system; (ii) a diversion of a small part of the photodetected signal from the slave interferometer (equipped with the 2D scanner head) towards the other inputs of the two mixers as used here (or more if extra master interferometers are added).

For up to a few MHz sweeping rate, where fast digitizer and parallel processing were demonstrated capable to deliver volumes in a few seconds or sub seconds, the add-on (employing a slow digitizer up to twice the sweeping frequency) can be used to deliver *en-face* OCT images based on downconversion in addition to the volumes and B-scan images delivered by a fast digitizer implementing FFT or MS (applied to GHz signals due to dense channeled spectra). For sweeping rates exceeding 10 MHz however, [6,15,16,17] the add-on will be the only block in the system providing images at the very step of acquisition (live), where the detailed volume can only be produced offline, later. The speed of the swept source here was 200 kHz, but the configuration is equally applicable to rates exceeding 10 MHz, as multi tens of GHz mixers exist of similar low cost to the mixers employed here (in fact even the active mixer used in this paper has a bandwidth exceeding 3 GHz). In other words, the online performance in delivering *en-face* OCT images demonstrated here is not restricted to tunning at 200 kHz, but will be online even at hundreds of MHz sweep rate.

So far, OCT investigations have mainly been focused on structural imaging via cross sections. A tool producing two or more *en-face* OCT images from different depths in real time did not exist. We hope that the instrument presented, to be used as such, or assembled as an add-on to any existing SSOCT flying spot system may find applications in the near future. If phenomena can be identified that are present at two or more depths simultaneously, then such an instrument could find unique applications not efficiently served by conventional cross sectioning OCT imaging. Possible directions of applications may be triggered by the recent attention given to pattern recognition in AI classification of diseases or material deformations.

Funding. European Commission (ITN GA GA860807 (NETLAS)); Imaging, Visual Assessment & Digital Innovation, at Moorfields Eye Hospital NHS FT and UCL Institute of Ophthalmology, University College London. (BRC, BRC3, BRC4-05-RB413-302); Biotechnology and Biological Sciences Research Council (5DHiResE (BB/S016643/1), BB/X003744/1); King's College and Moorfields Eye Hospital (NIHR 202879); MRC Impact Accelerator Account (project 18557); Development Pathway Funding Scheme (DPFS) MRC (662915); Engineering and Physical Sciences Research Council (26049, EP/X000125/1, FoVEnOCT).

Acknowledgments. RC, AMJ and AP thanks the ITN GA GA860807 (NETLAS), supported by the European Commission. RC and AP acknowledge the NIHR MOORFIELDS BRC, BRC3 and NIHR BRC4-05-RB413-302, Imaging, Visual Assessment & Digital Innovation, at Moorfields Eye Hospital NHS FT and UCL Institute of Ophthalmology. AP also acknowledges the UK's Biotechnology and Biological Sciences Research Council (BBSRC) for the research grants 5DHiResE (BB/S016643/1) and BB/X003744/1, as well as for the NIHR 202879 at King's College and Moorfields Eye Hospital, the MRC Impact Accelerator Account, project 18557 and the DPFS MRC 662915 to University of Nottingham

Optics EXPRESS

and University of Kent, the EPSRC, 26049, FoVEnOCT, EP/X000125/1. The authors also acknowledge the software created by Mark Hathaway for displaying two *en-face* images.

Disclosures. AP is inventor and coinventor of patents in the name of the University of Kent. No other conflict of interest.

Data availability. Data underlying this study are available from the authors upon reasonable request.

References

1. D. Huang, E. A. Swanson, C. P. Lin, *et al.*, "Optical Coherence Tomography," Science **254**(5035), 1178–1181 (1991).
2. S. R. Chinn, E. A. Swanson, and J. G. Fujimoto, "Optical coherence tomography using a frequency-tunable optical source," Opt. Lett. **22**(5), 340 (1997).
3. W. Drexler and J. G. Fujimoto, eds., *Optical Coherence Tomography: Technology and Applications* (Springer, 2008).
4. A. G. Podoleanu, "Optical coherence tomography," J. Microsc. **247**(3), 209–219 (2012).
5. W. Wieser, B. R. Biedermann, T. Klein, *et al.*, "Multi-Megahertz OCT: High quality 3D imaging at 20 million A-scans and 45 GVoxels per second," Opt. Express **18**(14), 14685 (2010).
6. A. M. Jimenez, S. Grelet, V. Tsatourian, *et al.*, "400 Hz Volume Rate Swept-Source Optical Coherence Tomography at 1060 nm Using a KTN Deflector," IEEE Photonics Technol. Lett. **34**(23), 1277–1280 (2022).
7. A. Podoleanu, R. Cernat, and A. Bradu, "Down-conversion en-face optical coherence tomography," Biomed. Opt. Expresss **10**(2), 772 (2019).
8. X. Attendu and R. M. Ruis, "Simple and robust calibration procedure for k-linearization and dispersion compensation in optical coherence tomography," J. Biomed. Opt. **24**(05), 1 (2019).
9. N. Huang, T. T. Hormel, G. B. Liang, *et al.*, "Optimizing numerical k-sampling for swept-source optical coherence tomography angiography," Opt. Lett. **49**(5), 1201 (2024).
10. A. Gh. Podoleanu and A. Bradu, "Master–slave interferometry for parallel spectral domain interferometry sensing and versatile 3D optical coherence tomography," Opt. Express **21**(16), 19324 (2013).
11. S. Rivet, M. Maria, A. Bradu, *et al.*, "Complex master slave interferometry," Opt. Express **24**(3), 2885 (2016).
12. R. Cernat, A. Bradu, N. M. Israelsen, *et al.*, "Gabor fusion master slave optical coherence tomography," Biomed. Opt. Expresss **8**(2), 813 (2017).
13. Di Nicola, Matteo Riccardo, Colombo Marco, *et al.*, "Scorpions: Taxonomy, anatomy, medical relevance, venom composition, pharmacology," Encyclopedia of Toxicology **1**, 445–456 (2024).
14. R. Mullen and W. David Sissom, "Chapter 23 - Scorpions," Medical and Veterinary Entomology (Third Edition) **1**, 489–504 (2019).
15. J. Xu, X. Wei, L. Yu, *et al.*, "High-performance multi-megahertz optical coherence tomography based on amplified optical time-stretch," Biomed. Opt. Express **6**(4), 1340–1350 (2015).
16. S. Tozburun, C. Blatter, M. Siddiqui, *et al.*, "Phase-stable Doppler OCT at 19 MHz using a stretched-pulse mode-locked laser," Biomed. Opt. Express **9**(3), 952–961 (2018).
17. X. Wei, A. K. S. Lau, Y. Xu, *et al.*, "28 MHz swept source at 1.0 μm for ultrafast quantitative phase imaging," Biomed. Opt. Express **6**(10), 3855–3864 (2015).